Supporting Information

Scaffold-Induced Diketopyrrolopyrrole Molecular Stacks in a Covalent Organic Framework

Sabrina Rager,[a] Andreas C. Jakowetz,[a] Bappaditya Gole,[b] Florian Beuerle,[b] Dana D. Medina[a]* and Thomas Bein[a]*

[a] Department of Chemistry and Center for NanoScience (CeNS), University of Munich (LMU), Butenandtstr. 5-13, 81377 Munich, Germany
[b] University of Würzburg, Institute of Organic Chemistry and Center for Nanosystems Chemistry (CNC), Am Hubland, 97074 Würzburg

E-mail: dana.medina@cup.uni-muenchen.de, bein@lmu.de
*Authors for correspondence

Table of Contents

1. Materials and methods

All applied materials (if not otherwise noted) were purchased from Aldrich or TCI in the common purities purum and puriss. All materials were used without further purification if not further noticed.

Powder X-ray diffraction (PXRD) measurements were performed on a Bruker D8 Discover diffractometer with Ni filtered Kα radiation (λ = 1.54060 Å) and a position-sensitive detector (LynxEye) in reflection mode. For high resolution measurements, the as synthesized COF material was placed on a silicon wafer and the measurement was carried out by applying a low scan speed.

Scanning electron microscopy (SEM) was performed on a FEI Helios G3 UC instrument at 2 kV. For this purpose, the samples were put on an adhesive graphite film and sputtered with carbon with a BALTEC MED 020 Coating System.

Transmission electron microscopy (TEM) data were obtained with a Tecnai G2 20 S-Twin instrument at an acceleration voltage of 200 kV.

Based on the symmetry of the applied building blocks, the final 2D COF structure can be approximately predicted and then confirmed with experimental powder X-ray diffraction (PXRD) data. The **simulation** was carried out with the visualization environment of Materials Studio software 4.4, and the geometry of the two-dimensional layers was optimized with calculations using forcite methods. Based on the geometry of the precursor molecules, the repeating unit was constructed in a unit cell of the P1 space group. The repeating fragments were placed in the triclinic unit cell and connected to each other, resulting in the complete unit cell. The geometry of the **DPP2-HHTP-COF** layer was optimized in the unit cell using the Dreiding forcefield and the QEq correction for weak interactions. Pawley refinements resulted in good values fitting our experimental PXRD data.

Nitrogen sorption was measured using a Quantachrome AUTOSORB 1 station at 77.3 K after degassing the sample for at least 12 h under vacuum at 150 °C. The Brunauer–Emmett–Teller (BET) surface area was calculated from the adsorption branch in the range of p/p_0 = 0.07–0.21. Pore sizes were calculated with a QSDFT adsorption model of N_2 on carbon (cylindrical, adsorption branch).

Thermogravimetric (TG) measurements were performed in a stream of synthetic air (25 ml / min) on a Netzsch STA 440 C TG/DSC instrument. The measurements were carried out with a heating rate of 10 °C / min, and a temperature range from 30 °C to 900 °C was covered.

^{1}H/^{13}C NMR solution spectra were recorded on a Bruker Avance III-400 MHz and a Bruker Avance III-270 MHz spectrometer. For this purpose, 4 mg of material were dissolved in characteristic deuterated solvents, respectively. Chemical shifts are reported in parts per million (ppm) with respect to residual $CHCl_3$ (0 ppm for ^{1}H and 77 ppm for ^{13}C) as the internal standard. Signal multiplicities are denoted as s (singlet), d (doublet), t (triplet), and m (multiplet).

The **IR-Spectra** were recorded on a Perkin Elmer Spectrum BX FT-IR instrument in combination with an attenuated total reflection (ATR) accessory comprising an ATR diamond crystal. All samples were measured at room temperature without further preparation.

UV-Vis spectra were recorded using a Perkin-Elmer Lambda 1050 spectrometer equipped with a 150 mm integrating sphere. The spectra were collected with a Praying Mantis (Harrick) accessory and were referenced to barium sulfate powder as white standard. The powder sample was mixed with a small amount of the reference and measured in diffuse reflectance mode.

Photoluminescence (PL) measurements were performed using a PicoQuant FluoTime300 **time-correlated single photon counting (TCSPC)** setup. The steady-state spectrum was recorded using a 378 nm laser (PicoQuant LDH-P-C-375), while TCSPC histograms and the time-resolved emission spectra (TRES) were acquired with 508 nm laser pulses (PicoQuant LDH-P-C-510) of 0.10 ns length and energy density of around 0.7 μJ/cm². In both cases, the emitted light was collected by a two-inch lens and focused onto a monochromator (Zolix Omni-λ 300). Residual scattered light from the excitation laser was removed using a 400 nm dielectric longpass (Thorlabs FELH0400) or a 3 mm orange glass filter (Schott OG530) for the 378 nm or 508 nm laser, respectively. The monochromatic light was detected under magic angle (54.7°) using a highly-sensitive photomultiplier (PicoQuant PMA 192).
We note that the steady-state PL spectra excited with 378 nm and 508 nm looked identical, but due to a larger spectral range, we chose the 378 nm spectrum in this study.

Hall conductivity measurements were carried out on an ECOPIA HMS 3000 apparatus using a magnetic field of 0.55 T in the Van der Pauw geometry connected by gold wires. The measurements were performed on pellets (10 mm diameter), which were prepared by pressing the finely ground materials (precursors and COF material) under a pressure of 0.75 to 1.2 GPa, respectively.

2. Structural characterization

Table S1: Refined crystal data for **DPP2-HHTP-COF**.

	DPP2-HHTP-COF
Chemical formula	$C_{11}H_{126}O_{18}B_6N_6S_6$
Formula weight	2269.64 g/mol
Crystal system	triclinic
Space group	*P*1 (1)
Unit cell dimension	*a*=43.82 Å *b*=44.57 Å *c*=3.48 Å α=89.79° β=89.53° γ=122.76°
Cell volume	5711.01 Å^3

Table S2: Atomic parameters for **DPP2-HHTP-COF**.

Atom	Atom label	x/a	y/b	z/c
N1	N	0.47822	0.44153	0.50000
C2	C	0.51432	0.46933	0.50000
C3	C	0.54376	0.46256	0.50000
S4	S	0.53744	0.42101	0.50000
C5	C	0.51747	0.50174	0.50000
C6	C	0.45834	0.45970	0.50000
O7	O	0.42581	0.44320	0.50000

C8	C	0.57845	0.48875	0.50000
C9	C	0.60049	0.47518	0.50000
C10	C	0.58188	0.43912	0.50000
B11	B	0.59987	0.41656	0.50000
O12	O	0.63787	0.43160	0.50000
O13	O	0.58032	0.37827	0.50000
C14	C	0.63990	0.40125	0.50000
C15	C	0.60763	0.37121	0.50000
C16	C	0.60280	0.33675	0.50000
C17	C	0.67072	0.40023	0.50000
C18	C	0.66893	0.36701	0.50000
C19	C	0.63494	0.33539	0.50000
H20	H	0.42478	0.68696	0.50000
H21	H	0.49348	0.86341	0.50000
H22	H	0.06807	0.58547	0.50000
H23	H	0.27132	0.69699	0.50000
N24	N	0.55847	0.03669	0.50000
C25	C	0.53067	0.04499	0.50000
C26	C	0.53744	0.08121	0.50000
S27	S	0.57899	0.11643	0.50000
C28	C	0.49826	0.01573	0.50000
C29	C	0.54030	0.99864	0.50000
O30	O	0.55680	0.98261	0.50000
C31	C	0.51125	0.08970	0.50000
C32	C	0.52482	0.12531	0.50000
C33	C	0.56088	0.14275	0.50000
B34	B	0.58344	0.18331	0.50000

O35	O	0.56840	0.20627	0.50000
O36	O	0.62173	0.20205	0.50000
C37	C	0.59875	0.23865	0.50000
C38	C	0.62879	0.23642	0.50000
C39	C	0.66325	0.26604	0.50000
C40	C	0.59977	0.27048	0.50000
C41	C	0.63299	0.30192	0.50000
C42	C	0.66461	0.29954	0.50000
H43	H	0.31304	0.73783	0.50000
H44	H	0.13659	0.63008	0.50000
H45	H	0.41453	0.48260	0.50000
H46	H	0.30301	0.57433	0.50000
C47	C	0.40260	0.93780	0.50000
C48	C	0.37678	0.89805	0.50000
C49	C	0.33809	0.88858	0.50000
C50	C	0.31303	0.84866	0.50000
C51	C	0.27423	0.83882	0.50000
C52	C	0.24305	0.80106	0.50000
C53	C	0.37013	0.86026	0.50000
C54	C	0.33149	0.83090	0.50000
H55	H	0.39250	0.94778	0.26106
H56	H	0.39032	0.94214	0.76346
H57	H	0.37678	0.89805	0.82268
H58	H	0.33282	0.90033	0.23793
H59	H	0.33252	0.89993	0.76346
H60	H	0.31839	0.83695	0.76175
H61	H	0.31789	0.83676	0.23654

H62	H	0.27046	0.85261	0.24657
H63	H	0.26850	0.85004	0.76346
H64	H	0.24666	0.78547	0.73554
H65	H	0.24168	0.78823	0.21549
H66	H	0.21772	0.80152	0.54897
H67	H	0.38344	0.85675	0.75950
H68	H	0.38237	0.85587	0.23654
H69	H	0.31958	0.82931	0.20914
H70	H	0.31644	0.83681	0.72266
H71	H	0.32984	0.80483	0.56820
N72	N	0.96331	0.52178	0.50000
C73	C	0.95501	0.48568	0.50000
C74	C	0.91879	0.45624	0.50000
S75	S	0.88357	0.46256	0.50000
C76	C	0.98427	0.48253	0.50000
C77	C	0.00136	0.54166	0.50000
O78	O	0.01739	0.57419	0.50000
C79	C	0.91030	0.42155	0.50000
C80	C	0.87469	0.39951	0.50000
C81	C	0.85725	0.41812	0.50000
B82	B	0.81669	0.40013	0.50000
O83	O	0.79373	0.36213	0.50000
O84	O	0.79795	0.41968	0.50000
C85	C	0.76135	0.36010	0.50000
C86	C	0.76358	0.39237	0.50000
C87	C	0.73396	0.39720	0.50000
C88	C	0.72952	0.32928	0.50000

C89	C	0.69808	0.33107	0.50000
C90	C	0.70046	0.36506	0.50000
H91	H	0.26217	0.57522	0.50000
H92	H	0.36992	0.50652	0.50000
H93	H	0.51740	0.93193	0.50000
H94	H	0.42567	0.72868	0.50000
C95	C	0.06220	0.46479	0.50000
C96	C	0.10195	0.47874	0.50000
C97	C	0.11142	0.44951	0.50000
C98	C	0.15134	0.46437	0.50000
C99	C	0.16118	0.43541	0.50000
C100	C	0.19894	0.44199	0.50000
C101	C	0.13974	0.50987	0.50000
C102	C	0.16910	0.50059	0.50000
H103	H	0.05222	0.44472	0.26106
H104	H	0.05786	0.44817	0.76346
H105	H	0.10195	0.47874	0.82268
H106	H	0.09967	0.43249	0.23793
H107	H	0.10007	0.43259	0.76346
H108	H	0.16305	0.48144	0.76175
H109	H	0.16324	0.48112	0.23654
H110	H	0.14739	0.41785	0.24657
H111	H	0.14996	0.41846	0.76346
H112	H	0.21453	0.46119	0.73554
H113	H	0.21177	0.45345	0.21549
H114	H	0.19848	0.41619	0.54897
H115	H	0.14325	0.52669	0.75950

H116	H	0.14413	0.52651	0.23654
H117	H	0.17069	0.49027	0.20914
H118	H	0.16319	0.47963	0.72266
H119	H	0.19517	0.52500	0.56820
N120	N	0.52178	0.55847	0.50000
C121	C	0.48568	0.53067	0.50000
C122	C	0.45624	0.53744	0.50000
S123	S	0.46256	0.57899	0.50000
C124	C	0.48253	0.49826	0.50000
C125	C	0.54166	0.54030	0.50000
O126	O	0.57419	0.55680	0.50000
C127	C	0.42155	0.51125	0.50000
C128	C	0.39951	0.52482	0.50000
C129	C	0.41812	0.56088	0.50000
B130	B	0.40013	0.58344	0.50000
O131	O	0.36213	0.56840	0.50000
O132	O	0.41968	0.62173	0.50000
C133	C	0.36010	0.59875	0.50000
C134	C	0.39237	0.62879	0.50000
C135	C	0.39720	0.66325	0.50000
C136	C	0.32928	0.59977	0.50000
C137	C	0.33107	0.63299	0.50000
C138	C	0.36506	0.66461	0.50000
H139	H	0.57522	0.31304	0.50000
H140	H	0.50652	0.13659	0.50000
H141	H	0.93193	0.41453	0.50000
H142	H	0.72868	0.30301	0.50000

C143	C	0.46479	0.40260	0.50000
C144	C	0.47874	0.37678	0.50000
C145	C	0.44951	0.33809	0.50000
C146	C	0.46437	0.31303	0.50000
C147	C	0.43541	0.27423	0.50000
C148	C	0.44199	0.24305	0.50000
C149	C	0.50987	0.37013	0.50000
C150	C	0.50059	0.33149	0.50000
H151	H	0.44472	0.39250	0.26106
H152	H	0.44817	0.39032	0.76346
H153	H	0.47874	0.37678	0.82268
H154	H	0.43249	0.33282	0.23793
H155	H	0.43259	0.33252	0.76346
H156	H	0.48144	0.31839	0.76175
H157	H	0.48112	0.31789	0.23654
H158	H	0.41785	0.27046	0.24657
H159	H	0.41846	0.26850	0.76346
H160	H	0.46119	0.24666	0.73554
H161	H	0.45345	0.24168	0.21549
H162	H	0.41619	0.21772	0.54897
H163	H	0.52669	0.38344	0.75950
H164	H	0.52651	0.38237	0.23654
H165	H	0.49027	0.31958	0.20914
H166	H	0.47963	0.31644	0.72266
H167	H	0.52500	0.32984	0.56820
N168	N	0.44153	0.96331	0.50000
C169	C	0.46933	0.95501	0.50000

C170	C	0.46256	0.91879	0.50000
S171	S	0.42101	0.88357	0.50000
C172	C	0.50174	0.98427	0.50000
C173	C	0.45970	0.00136	0.50000
O174	O	0.44320	0.01739	0.50000
C175	C	0.48875	0.91030	0.50000
C176	C	0.47518	0.87469	0.50000
C177	C	0.43912	0.85725	0.50000
B178	B	0.41656	0.81669	0.50000
O179	O	0.43160	0.79373	0.50000
O180	O	0.37827	0.79795	0.50000
C181	C	0.40125	0.76135	0.50000
C182	C	0.37121	0.76358	0.50000
C183	C	0.33675	0.73396	0.50000
C184	C	0.40023	0.72952	0.50000
C185	C	0.36701	0.69808	0.50000
C186	C	0.33539	0.70046	0.50000
H187	H	0.68696	0.26217	0.50000
H188	H	0.86341	0.36992	0.50000
H189	H	0.58547	0.51740	0.50000
H190	H	0.69699	0.42567	0.50000
C191	C	0.59740	0.06220	0.50000
C192	C	0.62322	0.10195	0.50000
C193	C	0.66191	0.11142	0.50000
C194	C	0.68697	0.15134	0.50000
C195	C	0.72577	0.16118	0.50000
C196	C	0.75695	0.19894	0.50000

C197	C	0.62987	0.13974	0.50000
C198	C	0.66851	0.16910	0.50000
H199	H	0.60750	0.05222	0.26106
H200	H	0.60968	0.05786	0.76346
H201	H	0.62322	0.10195	0.82268
H202	H	0.66718	0.09967	0.23793
H203	H	0.66748	0.10007	0.76346
H204	H	0.68161	0.16305	0.76175
H205	H	0.68211	0.16324	0.23654
H206	H	0.72954	0.14739	0.24657
H207	H	0.73150	0.14996	0.76346
H208	H	0.75334	0.21453	0.73554
H209	H	0.75832	0.21177	0.21549
H210	H	0.78228	0.19848	0.54897
H211	H	0.61656	0.14325	0.75950
H212	H	0.61763	0.14413	0.23654
H213	H	0.68042	0.17069	0.20914
H214	H	0.68356	0.16319	0.72266
H215	H	0.67016	0.19517	0.56820
N216	N	0.03669	0.47822	0.50000
C217	C	0.04499	0.51432	0.50000
C218	C	0.08121	0.54376	0.50000
S219	S	0.11643	0.53744	0.50000
C220	C	0.01573	0.51747	0.50000
C221	C	0.99864	0.45834	0.50000
O222	O	0.98261	0.42581	0.50000
C223	C	0.08970	0.57845	0.50000

C224	C	0.12531	0.60049	0.50000
C225	C	0.14275	0.58188	0.50000
B226	B	0.18331	0.59987	0.50000
O227	O	0.20627	0.63787	0.50000
O228	O	0.20205	0.58032	0.50000
C229	C	0.23865	0.63990	0.50000
C230	C	0.23642	0.60763	0.50000
C231	C	0.26604	0.60280	0.50000
C232	C	0.27048	0.67072	0.50000
C233	C	0.30192	0.66893	0.50000
C234	C	0.29954	0.63494	0.50000
H235	H	0.73783	0.42478	0.50000
H236	H	0.63008	0.49348	0.50000
H237	H	0.48260	0.06807	0.50000
H238	H	0.57433	0.27132	0.50000
C239	C	0.93780	0.53521	0.50000
C240	C	0.89805	0.52126	0.50000
C241	C	0.88858	0.55049	0.50000
C242	C	0.84866	0.53563	0.50000
C243	C	0.83882	0.56459	0.50000
C244	C	0.80106	0.55801	0.50000
C245	C	0.86026	0.49013	0.50000
C246	C	0.83090	0.49941	0.50000
H247	H	0.94778	0.55528	0.26106
H248	H	0.94214	0.55183	0.76346
H249	H	0.89805	0.52126	0.82268
H250	H	0.90033	0.56751	0.23793

H251	H	0.89993	0.56741	0.76346
H252	H	0.83695	0.51856	0.76175
H253	H	0.83676	0.51888	0.23654
H254	H	0.85261	0.58215	0.24657
H255	H	0.85004	0.58154	0.76346
H256	H	0.78547	0.53881	0.73554
H257	H	0.78823	0.54655	0.21549
H258	H	0.80152	0.58381	0.54897
H259	H	0.85675	0.47331	0.75950
H260	H	0.85587	0.47349	0.23654
H261	H	0.82931	0.50973	0.20914
H262	H	0.83681	0.52037	0.72266
H263	H	0.80483	0.47500	0.56820
C264	C	0.54923	0.59823	0.49535
H265	H	0.56677	0.60630	0.22361
H266	H	0.56697	0.60592	0.76082
C267	C	0.52703	0.61569	0.49683
H268	H	0.52703	0.61569	0.16902
C269	C	0.55525	0.65619	0.49206
H270	H	0.57402	0.66130	0.23690
H271	H	0.57297	0.66376	0.75755
C272	C	0.54976	0.68752	0.49119
H273	H	0.53164	0.68322	0.75000
H274	H	0.53394	0.68597	0.22524
C275	C	0.58024	0.72738	0.48622
H276	H	0.59864	0.73042	0.23525
H277	H	0.59774	0.73373	0.75178

C278	C	0.58099	0.76233	0.48454
H279	H	0.59530	0.77826	0.21196
H280	H	0.59620	0.77873	0.74706
H281	H	0.55201	0.75586	0.49336
C282	C	0.50239	0.63049	0.49869
H283	H	0.48275	0.61613	0.74971
H284	H	0.48453	0.62076	0.23332
C285	C	0.50898	0.66811	0.49628
H286	H	0.52095	0.68154	0.20597
H287	H	0.52872	0.68465	0.73380
H288	H	0.48215	0.66602	0.54729

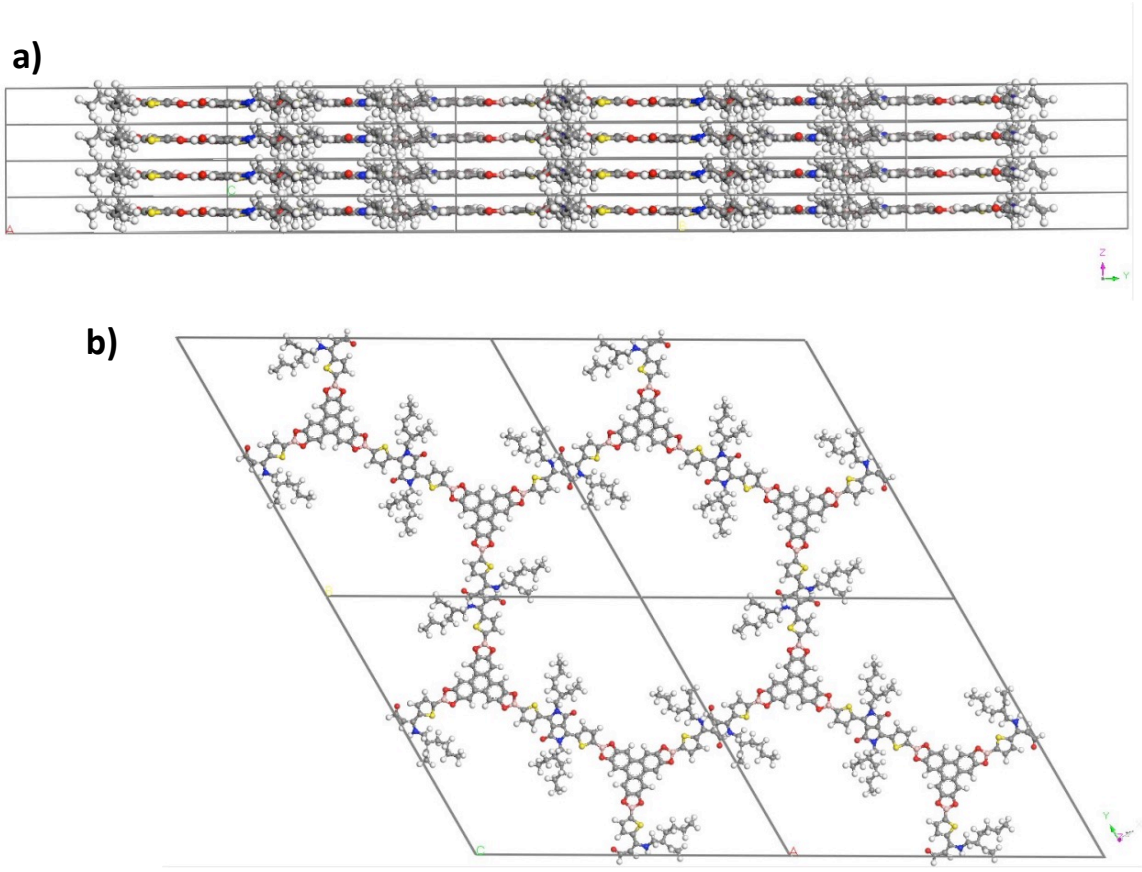

Fig. S1.1: a) side view of *P1* simulated crystal along the *y*-axis of 4 unit cells stacked on top of each other demonstrating the flat and rigid backbone consisting of **HHTP** and **DPP** including the distribution of the alkyl chains, b) Simulation of the crystal lattice of 4 unit cells in an eclipsed arrangement for **DPP2-HHTP-COF** illustrating the resulting pore shape, viewed along *z*.

Another possible space group for this system is space group *P6/mcc*, which includes the flipping of the eclipsed layers in one crystal unit cell. This possible arrangement was also calculated and illustrated in the figure below. In addition, the calculated PXRD patterns of the different space groups are compared to the experimental data. The simulated pattern for *P1* fits the experimental data well, whereas the pattern for *P6/mcc* is slightly shifted to smaller 2θ values. This is visualized by the vertical lines for the detected reflections in the experimental data.

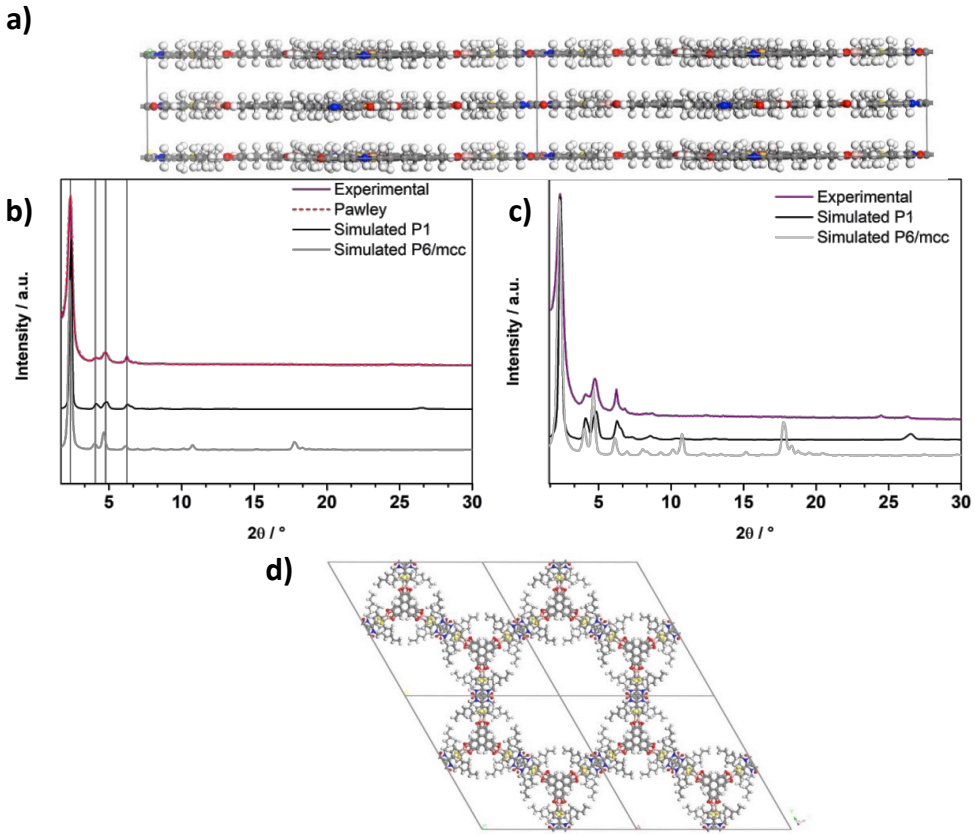

Fig. S1.2: a) simulation of the crystal unit cell in an eclipsed arrangement in the *P6/mcc* space group illustrating two flipped layers stacked on top of each other, b) Differences between the calculated patterns for space groups *P1* (black) and *P6/mcc* (grey) in comparison to the experimental data (purple) and the corresponding Pawley refinement (red dashed), c) PXRD pattern of experimental data (purple), and simulated in *P1* (black) and *P6/mcc* (grey) in logarithmic scale, d) top view on AB plane for the *P6/mcc* space group.

3. Synthesis of precursor DPP2

Compounds (**Ethex)$_2$-DPP**[1] and (**Bpin)$_2$-DPP**[2] were synthesized according to literature procedures and structural identity was proven by comparing ^{1}H-NMR data to literature reports.

Synthesis of racemic 2,5-bis(2-ethylhexyl)-3,6-di(thiophen-2-yl)-2,5-dihydropyrrolo[3,4-c]pyrrole-1,4-dione **(Ethex)$_2$-DPP**)[1]

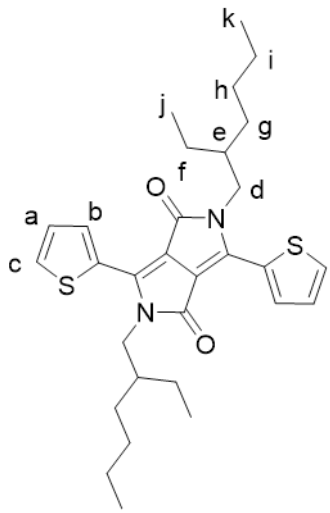

Molecular Weight: 524,78

In a three-necked flask, 3,6-di(thiophen-2-yl)-2,5-dihydropyrrolo[3,4-c]pyrrole-1,4-dione (**DPP**) (2.52 g, 8.4 mmol, 1 eq.) and potassium carbonate (6.6 g, 48 mmol, 3 eq.) were dissolved in DMF (120 mL). The mixture was heated to 120 °C for one hour and racemic 2-ethylhexyl bromide (8.5 mL, 48 mmol, 3 eq.) was added dropwise. The reaction mixture was then stirred for 48 hours at 120 °C. The temperature was increased to 150 °C for the last four hours. After cooling down, the solvent was reduced *in vacuo*. The dark purple residue was then dissolved in CH_2Cl_2 (300 mL) and washed with water (3 x 150 mL) and saturated brine (2 x 150 mL). The combined aqueous phases were extracted with CH_2Cl_2 (2 x 100 mL). The organic phases were dried over Na_2SO_4 and the solvent was removed under reduced pressure. The crude product was subsequently purified by column chromatography on silica gel (CH_2Cl_2 / pentane 50:50, later increased to 80:20) to afford the product as a dark red powder (1.26 g, 2.40 mmol, 30 %).

^{1}H NMR (400 MHz, $CDCl_3$, rt): δ = 8.89 (dd, ^3J = 3.9, ^4J = 1.2 Hz, 2H, H_c), 7.63 (dd, ^3J = 5.0, ^4J = 1.2 Hz, 2H, H_b), 7.27 (dd, ^3J = 5.0, 3.9 Hz, 2H, H_a), 4.08-3.97 (m, 4H, H_d), 1.90-1.79 (m, 2H, H_e), 1.40-1.18 (m, 16H, $H_{f\text{-}i}$), 0.90-0.82 (m, 12H, $H_{j\text{-}k}$) ppm.

Synthesis of 2,5-bis(2-ethylhexyl)-3,6-bis(5-(4,4,5,5-tetramethyl-1,3,2-dioxaborolan-2-yl)-thiophen-2-yl)-2,5-dihydropyrrolo[3,4-c]pyrrole-1,4-dione **(Bpin)$_2$-DPP**)[2]

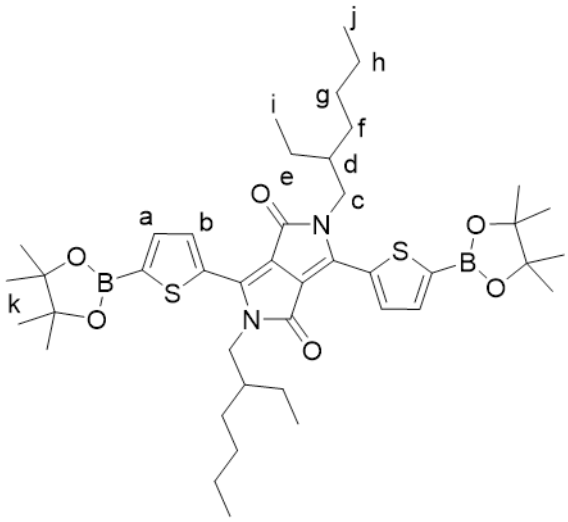

Molecular Weight: 776,71

(EtHex)$_2$-DPP (286 mg, 0.545 mmol, 1 eq.) was dissolved in THF (40 mL) in a Schlenk flask under inert gas. The mixture was cooled down to −78 °C and LDA solution (0.375 M in THF, 2.18 mL, 0.818 mmol, 1.5 eq.) was added dropwise. After stirring for two hours at the low temperature, isopropoxyboronic acid pinacol ester (0.165 mL, 0.818 mmol, 1.5 eq.) was added. Afterwards, the solution was allowed to warm up to room temperature and stirred for another two hours. The mixture was then poured into ice water (100 mL) followed by extraction with CH_2Cl_2 (2 x 100 mL) and $CHCl_3$ (2 x 100 mL). The combined organic phases were washed with saturated $NaHCO_3$ solution (2 x 100 mL) and brine (2 x 100 mL) and dried over Na_2SO_4. The solvents were removed under reduced pressure and the crude product was washed with hexane (5 mL) to yield the desired product as a red solid in sufficient purity (220 mg, 0.28 mmol, 52 %).

^{1}H NMR (400 MHz, $CDCl_3$, rt): δ = 8.92 (d, ^{3}J = 3.9 Hz, 2 H, H_a), 7.71 (d, ^{3}J = 3.9 Hz, 2H, H_b), 4.13-4.00 (m, 4H, H_c),1.88-1.80 (m, 2H, H_d), 1.40-1.18 (m, 16 H, H_{e-h}), 1.37 (s, 24 H, H_k) 0.90-0.82 (m, 12H, H_{i-j}) ppm.

Synthesis of ((2,5-bis(2-ethylhexyl)-3,6-dioxo-2,3,5,6-tetrahydropyrrolo[3,4-c]-pyrrole-1,4-diyl)bis(thiophene-5,2-diyl))diboronic acid (**DPP2**)

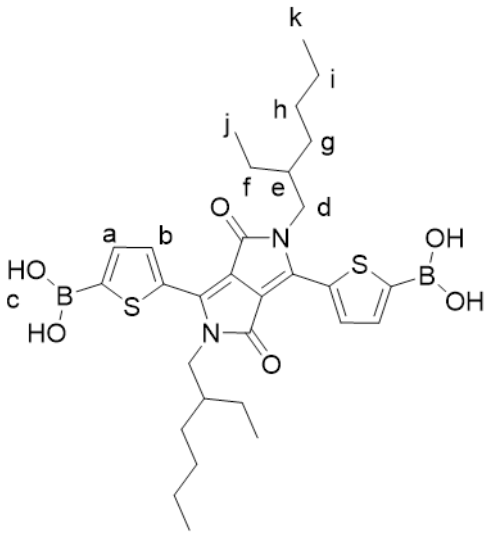

Molecular Weight: 612,41

(Bpin)$_2$-DPP (57.3 mg, 73.4 µmol, 1 eq.) was dissolved in a small amount of THF (0.5 mL). Water (2.5 mL) was added and the solution was stirred for two hours. Then, 6-molar hydrochloric acid (2.5 mL) was added and the mixture was stirred overnight at room temperature. Water (25 mL) was added and stirring was continued for two hours whereupon a dark red precipitate emerged while the solution became clear. The precipitate was filtered and washed with CH_2Cl_2 (2 x 5 mL) to afford the title compound as a shining red solid which was dried for eight hours under high vacuum (34.4 mg, 56.2 µmol, 77 %).

IR: 3358 (s), 2955 (w), 2930 (w), 2194 (vw), 2096 (vw), 2054 (vw), 1601 (vs), 1581 (vs), 1512 (m), 1443 (m), 1408 (s), 1368 (m), 1324 (vs), 1288 (m), 1254 (w), 1222 (w), 1125 (s), 1083 (s), 1032 (m), 919 (vw), 817 (m), 742 (m), 711 (m), 683 (w), 657 (w).

^{1}H NMR (400 MHz, THF-d_6, rt): δ = 9.11 (d, ^{3}J = 3.8 Hz, 2H, H_a), 7.67 (d, ^{3}J = 3.8 Hz, 2H, H_b), 7.67 (s, 4H, H_c), 4.16-4.05 (m, 4H, H_d), 1.97-1.89 (m, 2H, H_e), 1.42-1.22 (m, 16H, H_{f-i}), 0.92-0.84 (m, 12H, H_{j-k}) ppm.

^{13}C NMR (100 MHz, DMSO-d_6, rt): δ = 160.82, 139.83, 136.37, 135.30, 133.74, 107.26, 67.04, 30.44, 29.59, 27.76, 25.15, 23.22, 22.37, 13.78, 10.29 ppm.

4. Synthesis of DPP2-HHTP-COF

Extensive screening of the reaction conditions led to the following optimized synthesis procedure for **DPP2-HHTP-COF**. We note that the high concentration in the reaction mixture is crucial for obtaining high yield and high crystallinity. Furthermore, the framework also forms by allowing for increased reaction time (160 hours) with the adverse effect of reduced crystallinity (**DPP2-HHTP-COF** amorphous).

A 10 mL Schott Duran glass was charged with **DPP2** (25.02 mg, 0.153 mmol, 4 eq.) and 2,3,6,7,10,11-hexahydroxytriphenylene (**HHTP**) (11.8 mg, 0.039 mmol, 1 eq.). The solvent mixture consisting of mesitylene and dioxane at the ratio 1:1 was added to the powder (1 mL). This reaction mixture was sonicated for one minute to achieve a homogenous dispersion and further heated at 100 °C for 24 hours. The reddish purple solid was isolated by filtration and washed with dry acetone (2 x 5 mL). Finally, **DPP2-HHTP-COF** was obtained as dark purple powder (73%).

Furthermore, the amorphous **DPP2-HHTP-COF** was synthesized in a procedure similar to that for the crystalline material but with another solvent ratio and using an increased reaction time. To the same weights of the precursors, a solvent mixture of mesitylene and ethanol in the ratio of 1.5:1 was added (1 mL) and the reaction mixture was placed at 120 °C for 160 hours.

5. Characterization of DPP2-HHTP-COF material

The successful formation of the boronate ester-linked **DPP2-HHTP-COF** was confirmed by IR-spectroscopy (see Fig. S2a). The characteristic B-O stretching mode at 1347 cm^{-1} and the C-O stretching mode at 1240 cm^{-1} indicate the coupling of the precursors. Moreover, the characteristic O-H vibration is still visible around 3300 cm^{-1} due to the existence of hydroxyl groups at the outer surface of the COF material arising from the **HHTP** precursor.

IR: 3960 (vw), 3633 (vw), 3327 (m), 2957 (m), 2927 (w), 2181 (vw), 1639 (vs), 1564 (m), 1509 (m), 1441 (s), 1394 (s), 1347 (vs), 1290 (vs), 1285 (vs), 1240 (s), 1159 (m), 1102 (s), 1067 (s), 1028 (s), 966 (m), 868 (w), 828 (w), 736 (m), 722 (w), 722 (m), 678 (vw), 657 (vw).

The TGA analysis of **DPP2-HHTP-COF** illustrated in Fig. S2b indicates a complete removal of volatile guest molecules at about 170 °C (I). The subsequent mass loss of about 20 % (II) is proposed to relate to the loss of the solubilizing branched alkyl chains. The further degradation of the framework starts at around 400 °C (III) and the remaining amount of 10 wt% (IV) corresponds to approximately 3 mol B_2O_3, related to the sample weight.

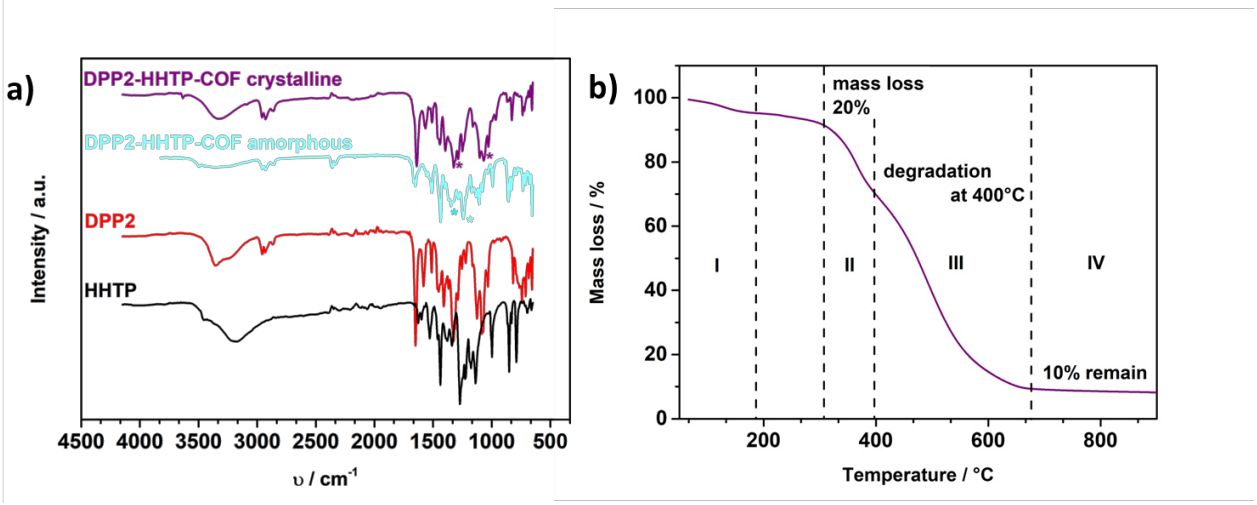

Fig. S2: a) IR spectra of **DPP2-HHTP-COF** illustrating the formation of the framework by marking the typical boronate ester vibrations with a star; **DPP2-HHTP-COF crystalline** (purple), **DPP2-HHTP-COF amorphous** (light blue), **DPP2** precursor (red) and **HHTP** precursor (black); the vibration at around 3400 cm^{-1} is attributed to the remaining hydroxyl groups of the **HHTP** counterpart. b) TGA data of **DPP2-HHTP-COF**.

6. Preparation of COF pellets for conductivity measurements

Table S3: Overview of the different materials prepared for subsequent Hall measurements.

Sample name	**Sample number**	**Applied pressure / GPa**	**Pellet thickness / µm**
DPP	1-5	0.85	190
DPP2	1-4	0.80	170
Crystalline **DPP2-HHTP-COF** pellet	1	0.75	240
	2	0.75	260
	3	0.70	190
	4	0.80	250
	5	0.80	70
	6	0.75	140
	7	0.90	190
	8	0.90	120
	9	1.20	120
	10	1.20	320
	11	1.20	150
	12	1.15	180
	13	1.15	160
	14	0.90	130
	15	1.15	220
Amorphous **DPP2-HHTP-COF** pellet	1	1.20	130
	2	1.20	130
	3	1.20	410
	4	1.25	320
	5	1.20	180

The crystallinity of the different pellets is illustrated in Fig. S3, which shows that crystallinity is preserved. The slightly lower crystallinity compared to the as-synthesized powder is attributed to the effect of the applied pressure (see Table S3). The amorphous COFs were treated referred to Table S3 and no higher crystallinity could be observed.

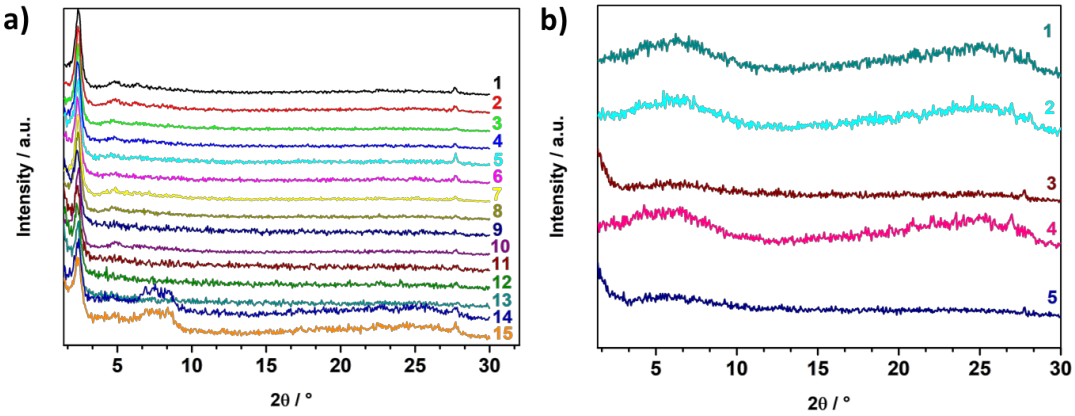

Fig. S3: XRD measurements for a) crystalline pellets of **DPP2-HHTP-COF** and b) amorphous pellets of **DPP2-HHTP-COF** (see Table S 3).

7. Conductivity measurements (Hall measurements)

Hall measurements were carried out in the Van der Pauw geometry. The pellet thickness was determined by using a sliding caliper.

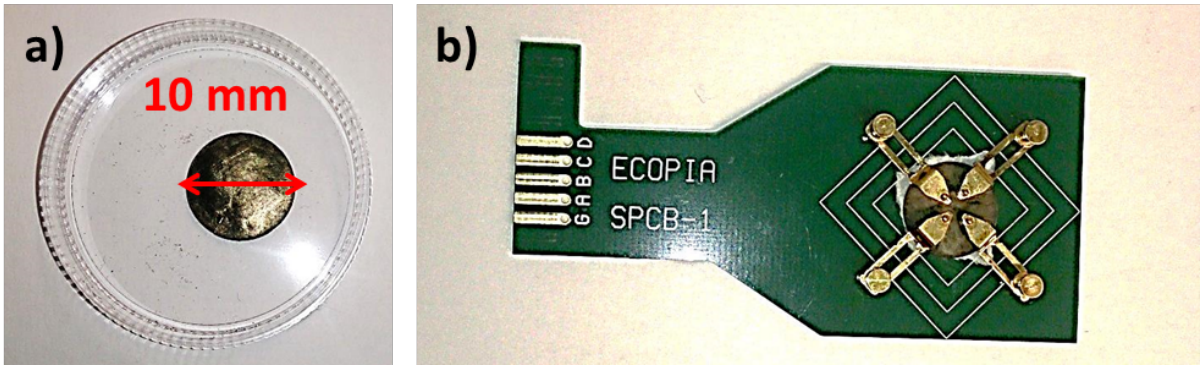

Fig. S4: a) Illustration of the 10 nm diameter **DPP2-HHTP-COF** pellet and b) construction of the Hall measurement setup in the Van der Pauw geometry.

Table S4: Results for Hall measurements on precursor pellets.

Precursor pellet	Average conductivity / S cm^{-1}
DPP	6.81×10^{-08}
DPP2	1.33×10^{-08}

Table S5: Results for Hall measurements on crystalline **DPP2-HHTP-COF** pellets.

Crystalline **DPP2-HHTP-COF** pellet	Conductivity / S cm^{-1}
1	4.99×10^{-08}
2	1.72×10^{-08}
3	1.08×10^{-07}
4	7.32×10^{-08}
5	1.11×10^{-07}
6	4.99×10^{-08}
7	2.20×10^{-06}
8	7.21×10^{-07}
9	5.66×10^{-08}
10	7.12×10^{-08}
11	3.52×10^{-08}
12	7.02×10^{-08}
13	2.15×10^{-08}
14	4.29×10^{-08}
15	8.52×10^{-08}

Table S6: Results for Hall measurements on amorphous **DPP2-HHTP-COF** pellets.

Amorphous **DPP2-HHTP-COF** pellet	Conductivity / S cm^{-1}
1	1.96×10^{-07}
2	2.47×10^{-07}
3	1.26×10^{-07}
4	1.89×10^{-07}
5	2.07×10^{-07}

8. Steady-state and time-resolved optical characterization

8.1. Crystalline and amorphous DPP2-HHTP-COF

To better assign the spectral features in the emission spectra of **DPP2-HHTP-COF**, we first investigated the precursors both in solution and as a solid film, i.e. in its aggregated form. The measured transmission UV-Vis spectra are shown in Figure S5a and PL spectra can be found in Figure S5b. The absorption shows two distinct peaks with the largest feature at around 565 nm for **DPP2** in solution (acetone, chloroform, and ethanol) and a peak at 572 nm in the solid thin film of **DPP2**. The overall red-shift of the film spectrum is attributed to a formation of *J*-type interactions within the molecular stacks. While the spectra of **DPP2** in acetone, ethanol, and chloroform exhibit the main peak at around 580 nm, the solid film of **DPP2** exhibits a main peak at 585 nm and the spectrum is red-shifted again. Furthermore, the overall spectral shapes of the film, with the strongest peak being the first peak just above the absorption gap (in energy), supports the formation of *J*-aggregates rather than *H*-aggregates where the second peak gets promoted in classical Kasha-theory.

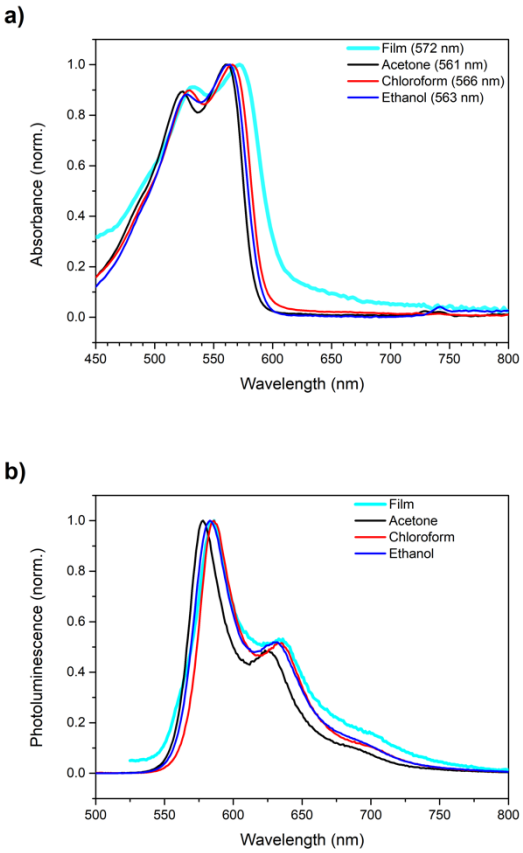

Fig. S5: Transmission UV-Vis a) and photoluminescence b) spectra of **DPP2** as precursor in solution (thin lines) and as a film (thick line). The values in the legend of a) indicate the position of the largest peak.

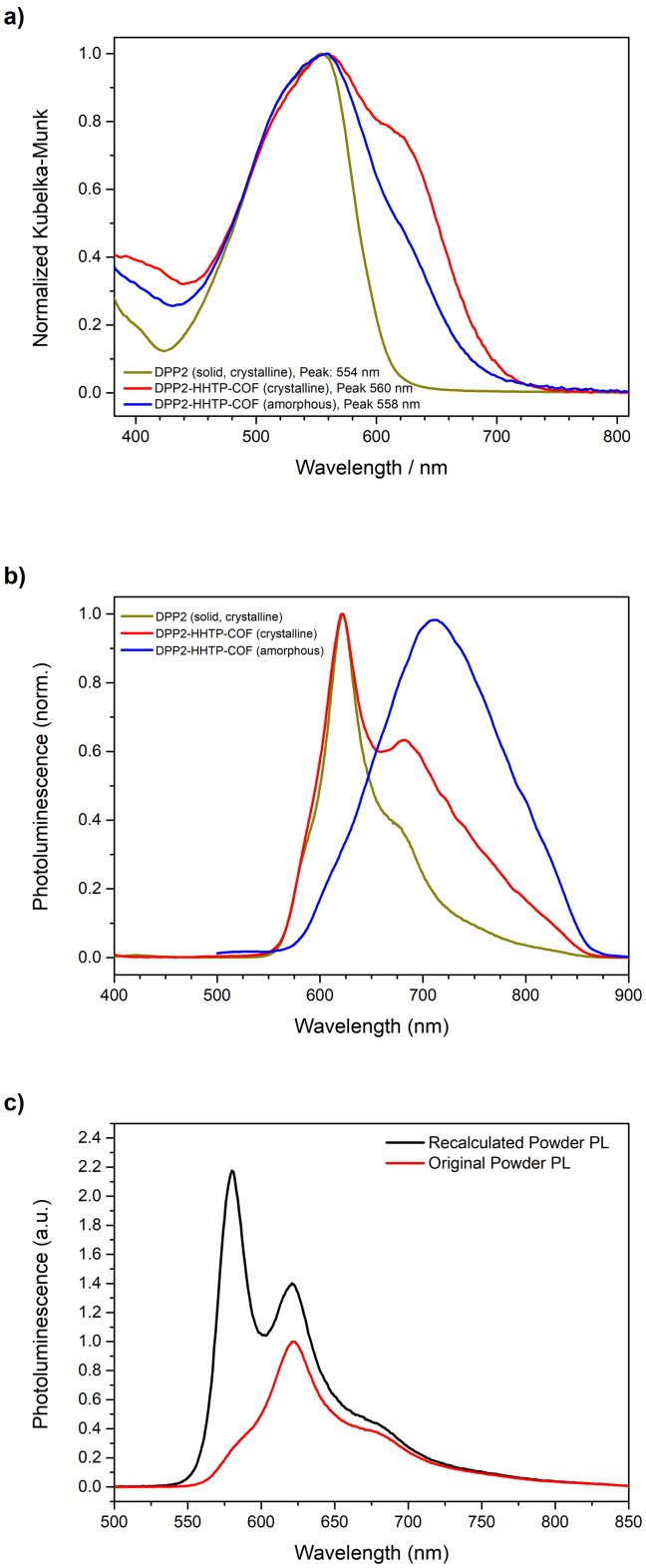

Fig. S6.1: Diffusive reflectance absorption a) and photoluminescence b) spectra of solid **DPP2** and **DPP2-HHTP-COF** (crystalline and amorphous). The values in the legend of (a) indicate the position of the largest peak. c) Photoluminescence spectrum of solid **DPP2** precursor as a powder (red line) and a qualitative recalculation of the emission spectrum without self-absorption (black line).

The absorption and PL emissions of crystalline and amorphous **DPP2-HHTP-COF** powders are shown in Figure S6.1a and b, together with the spectra of solid **DPP2** as powder. The comparison between crystalline solid precursor and COF (crystalline and amorphous) in Figure S6.1a clearly shows a strong extension of the absorption into the red for the crystalline COF. We note that in the PL (b) the spectral difference between the **DPP2** powder and the film is caused by the very different sampling volume. In the film, the emission is collected from a thin film (order of 100 nm) while in the powder, the light is fully absorbed by the **DPP2** crystallites (>10 µm scale). Hence, the emission from regions inside the crystallites is self-absorbed by the outer layers and hence the first peak around the HOMO-LUMO difference is truncated. The **DPP2** spectrum can be recalculated qualitatively through the UV-Vis of the **DPP2** film (Figure S6.1c), however absolute values are difficult to determine due to the too large thickness of the crystallites. Since the **DPP2-HHTP-COF** can only be measured as a powder, we use the powder **DPP2** data for the following comparison in order to have the same sampling volume. While the amorphous **DPP2-HHTP-COF** exhibits one broad peak, the crystalline **DPP2-HHTP-COF** shows an additional peak at around 620 nm, which is also observed in the **DPP2** solid, which from the film measurements show molecular stacks with *J*-type interaction. Since crystalline and amorphous COFs are synthesized in similar steps and conditions, this additional peak might be attributed to a similarly arranged stack of **DPP** as part of the COF framework, i.e. the 2D sheets arrange in such a way that the **DPP2** linker forms *J*-type interactions across the stacked sheets. Notably, if the peak had originated from molecular **DPP2** aggregates within the pore system, a much smaller framework surface area and pore size distribution should have been observed. XRD measurements also show that there are no detectable amounts of residual precursor **DPP2** in the sample – especially not in an amount that would generate this well-pronounced peak in the emission spectrum. We note that the slightly slipped stacking arrangement of the COF will most likely not result in *J*-aggregates as in Kasha's picture but rather in molecular stacks with *J*-type interaction when taking charge transfer into account as by Hestand and Spano.[3]

We note that in a slip stack assembly, two displacements are possible; along the short and the long axis of the dye as sketched in Figure S6.2. According to Hestand & Spano, small shifts of about 1.4 Å along either short or long axis of the building block can result in a *J*-type interaction in perylene aggregates (as compared to around 5.5 Å shift along the long axis required for a Kasha *J*-aggregate).

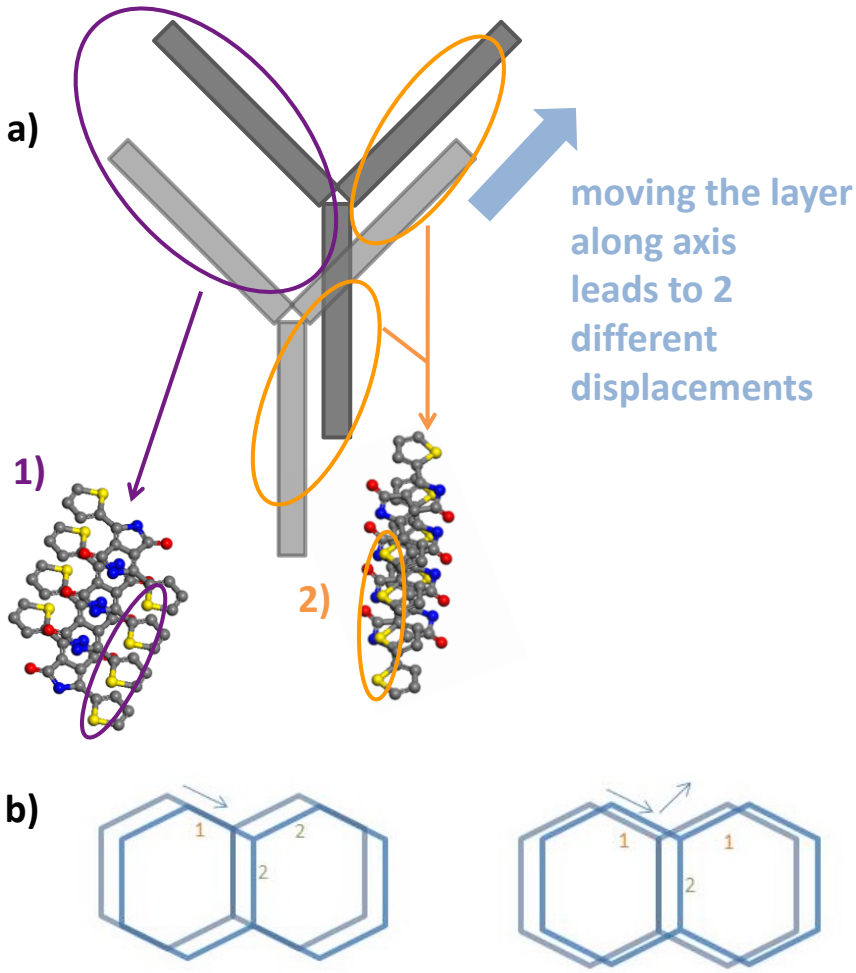

Fig. S6.2: a) Fragment of the hexagonal framework to illustrate possible displacement in a hexagonal pore. Linker molecules are represented and simplified by grey rectangles while dark and bright shading illustrates to neighboring layers. This results in two different DPP aggregation types regarding the position of the sulfur atoms: 1) sulfur placed in front of the previous atom, i.e. displacement along short axis of linker molecule (purple); 2) sulfur located next to the atom of the adjacent layer, i.e. displacement along long axis of linker molecule (orange). b) Two possible layer-to-layer offsets of the overall hexagonal pattern, showing that, in any case, there are always two different displacements yielding two well-defined aggregation types 1 and 2.

Assuming the requirement of similar displacements in our COF system, i.e. of around 1.4 Å, we simulated a corresponding slip-stack model with α = 68°. The simulated X-ray diffraction pattern refined for line broadening due to small COF domains could, within the limits, successfully reproduce the experimental XRD pattern (see Figure S6.3) and therefore leads to a consistent interpretation concerning the correlation between structural features and spectroscopic signatures in the COF. Notably, PXRD was refined for line broadening assuming spherical COF crystallites of 30 nm in size according to the TEM analysis.

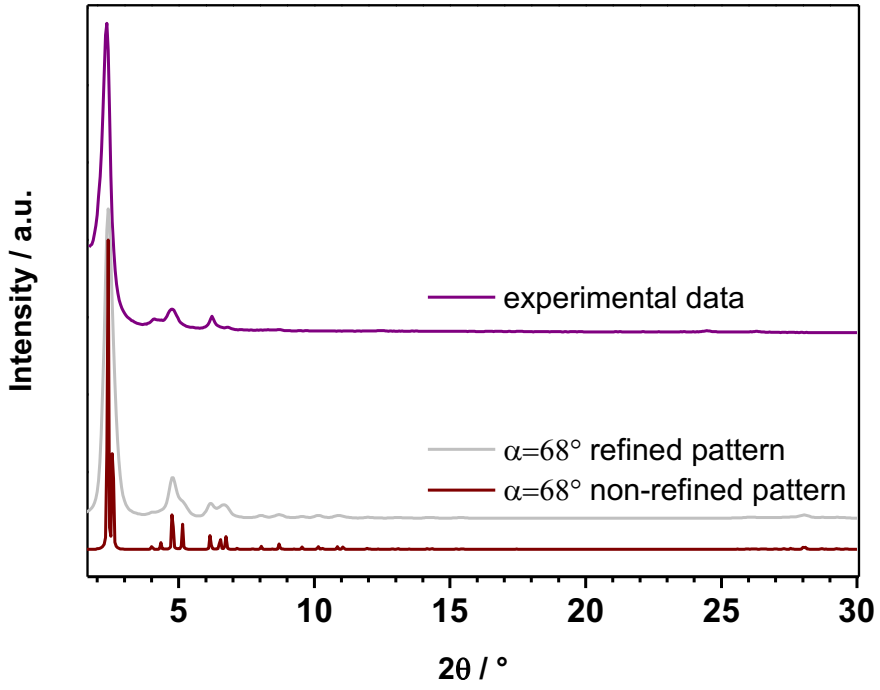

Fig. S6.3: Experimental powder XRD data of the **DPP2-HHTP-COF** (purple). Simulated XRD pattern for the P1 unit cell with parameters as those given in Table S1, except of alpha which is set to 68° (deep red), with the patterns refined to a crystal diameter of 30 nm (grey).

8.2. TCSPC measurements on crystalline DPP2-HHTP-COF

The comparison between time-correlated single photon counting (TCSPC) decays at 620 nm and 680 nm measured on the crystalline **DPP2-HHTP-COF** sample can be found in Figure S7. The corresponding results of triexponential fits can be found in Table S7 with short, medium, and long timescales τ_1, τ_2, and τ_3, respectively. We note that the given uncertainties are fitting errors and are for most of the results much smaller than the actual instrument response time. The latter is mainly determined through the laser pulse length and is around 0.10 ns. To illustrate the much faster instrument response, it is shown together with the **DPP2-HHTP-COF** data in Figure S8. From the direct comparison of the decays at 620 nm and 680 nm, we see that all three timescales of the triexponential fits are very similar. The emission at 680 nm shows slightly larger values for τ_1 and τ_2 and a higher contribution of τ_2 to the overall intensity. While the 620 nm emission exhibits the largest value of τ_3 of 5.6 ns, it has to be noted that the values for 620 nm and 680 nm both have a relatively large error and match within their combined error margin.

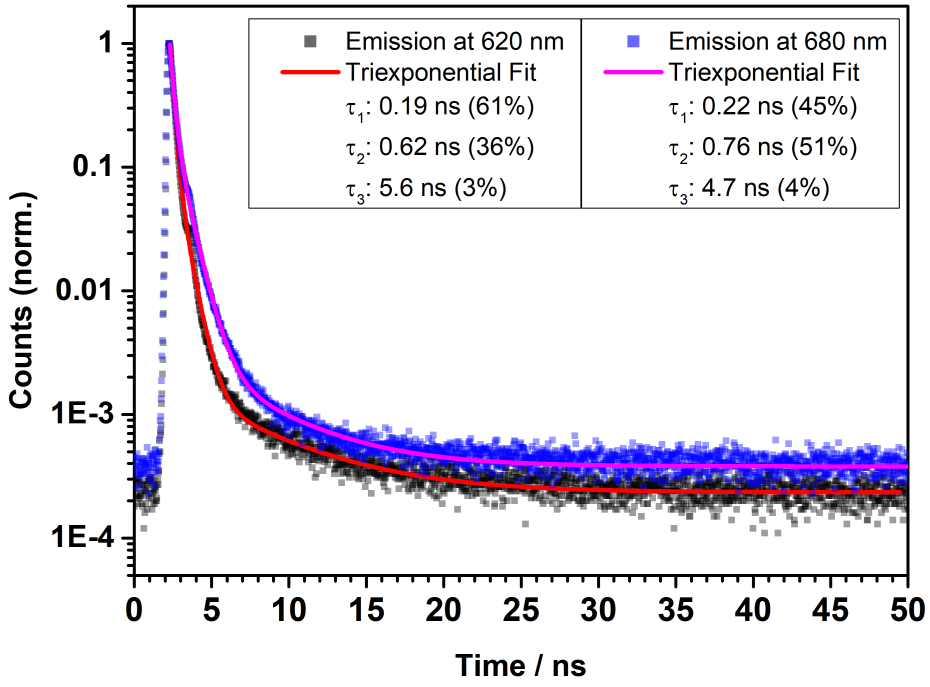

Fig. S7: TCSPC decays of crystalline **DPP2-HHTP-COF** at both distinct peaks of the PL spectrum, i.e. at 620 nm (black squares) and 680 nm (blue squares). The corresponding triexponential fits are given as solid lines in red and magenta for the 620 nm and 680 nm data, respectively.

Table S7: Fitting results of the triexponential fits to the respective TCSPC datasets of the crystalline **DPP2-HHTP-COF** (see Figure S7). We note that uncertainties are fitting errors and, partly, much smaller than the instrument response of around 0.10 ns.

	620 nm	Fractional intensity	680 nm	Fractional intensity
τ_1	(0.190 ± 0.004) ns	61%	(0.223 ± 0.004) ns	45%
τ_2	(0.619 ± 0.011) ns	36%	(0.760 ± 0.008) ns	51%
τ_3	(5.6 ± 0.5) ns	3%	(4.7 ± 0.3) ns	4%

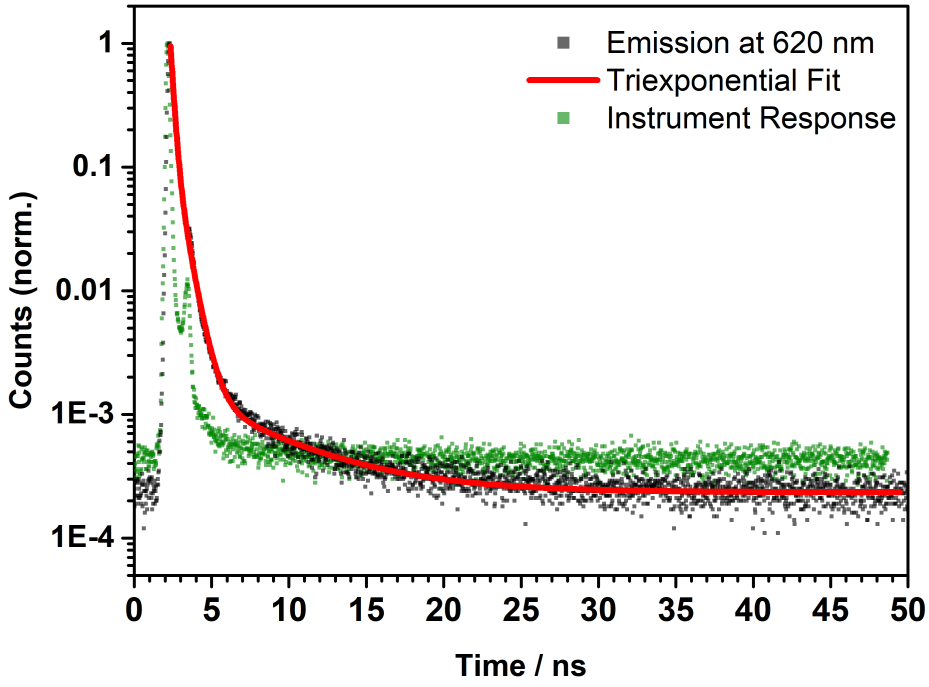

Fig. S8: TCSPC decay of crystalline **DPP2-HHTP-COF** at 620 nm (black squares) and the instrument response of the 508 nm laser (green squares).

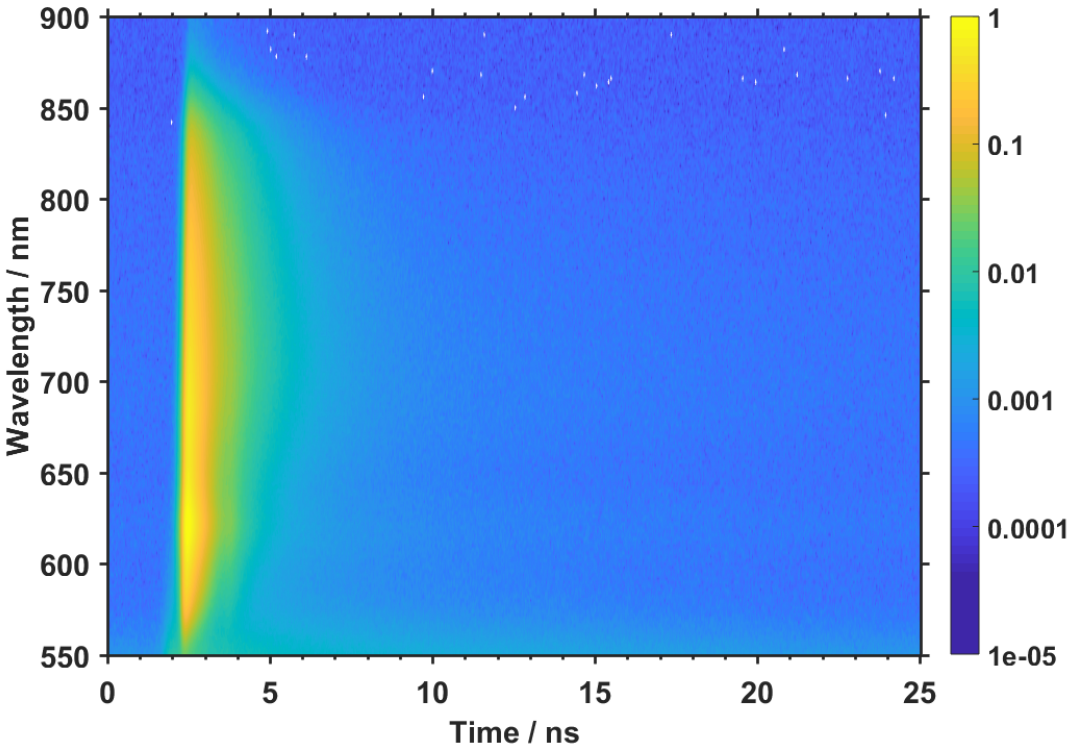

Fig. S9: Time-resolved emission spectra (TRES) of crystalline **DPP2-HHTP-COF**. The data are normalized to the main peak and the color scale is logarithmic.

8.3. TCSPC measurements on amorphous DPP2-HHTP-COF

Figure S10 contains a direct comparison between crystalline and amorphous **DPP2-HHTP-COF** samples regarding their time-resolved PL decays. Here, for both samples, the decay was probed within the broad emission feature, which both samples have in common. For the crystalline material, it was monitored at 680 nm while for the amorphous sample, the peak at 705 nm was used. As in the previous section, the datasets were fitted with triexponential functions with short, medium, and long timescales τ_1, τ_2, and τ_3, respectively. The fitting results are summarized in Table S8.

We see that both decays exhibit the same timescales, i.e. the same within their error margins. Furthermore, the contributions to the overall decay intensities of the three timescales are also very similar. From this observation and the similarity in their broad PL feature, we relate this emission to a state generated through the COF formation, while the specific origin would require further investigation and is not part of this study.

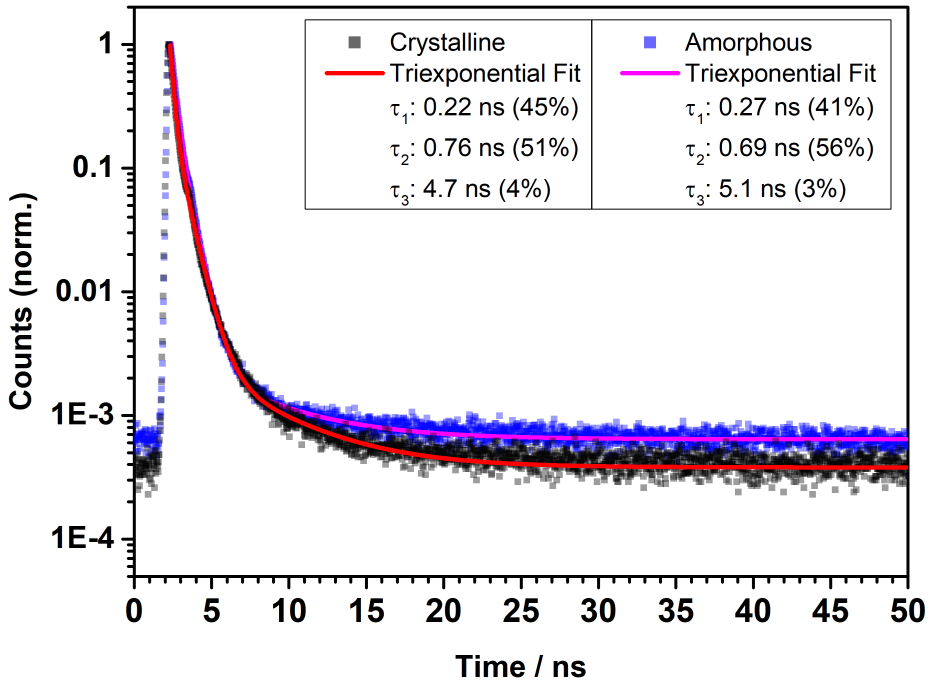

Fig. S10: TCSPC decays of crystalline and amorphous **DPP2-HHTP-COF** at 680 nm (black squares) and at 705 nm (blue squares), respectively. The corresponding triexponential fits are given as solid lines in red and magenta for the crystalline and amorphous samples, respectively.

Table S8: Fitting results of the triexponential fits to the respective TCSPC datasets of the crystalline and amorphous **DPP2-HHTP-COF** (see Figure S12). We note that uncertainties are fitting errors and, partly, much smaller than the instrument response of around 0.10 ns.

	Crystalline **DPP2-HHTP-COF**	Fractional intensity	Amorphous **DPP2-HHTP-COF**	Fractional intensity
τ_1	(0.223 ± 0.004) ns	45%	(0.267 ± 0.005) ns	41%
τ_2	(0.760 ± 0.008) ns	51%	(0.694 ± 0.006) ns	56%
τ_3	(4.7 ± 0.3) ns	4%	(5.1 ± 0.4) ns	3%

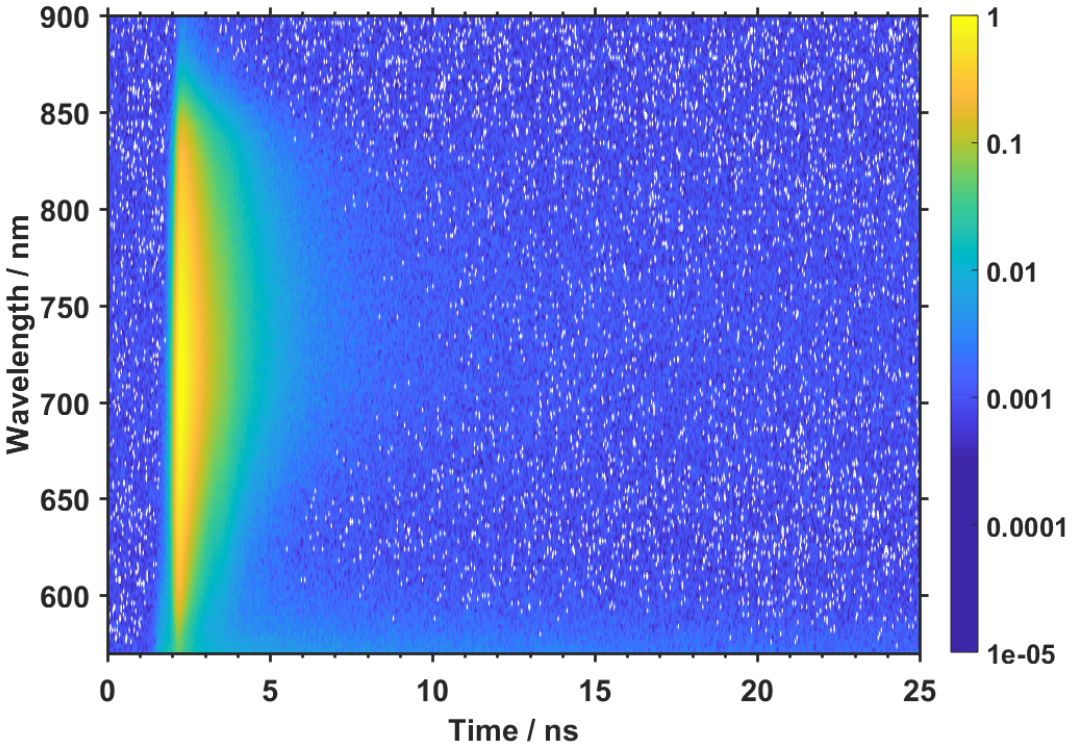

Fig. S11: Time-resolved emission spectra (TRES) of amorphous **DPP2-HHTP-COF**. The data is normalized to the main peak and the color scale is logarithmic.

8.4. Photoluminescence of DPP2 and HHTP precursors

Figure S12 shows the PL spectra of solid powder **DPP2** and solid HHTP precursors. While the former has already been discussed in Section S8.1, the latter is shown here for the sake of completeness. The main PL peak of HHTP is further to the blue spectral region than the observed PL of the COF materials. Therefore, we conclude that HHTP aggregates do not play a role in the COF emission, unlike the **DPP2,** and that no residual HHTP can be observed either. This is supported by the long lifetimes observed in the COF, which are much larger than the 1.0 ns decay component of the solid HHTP (see Figure S13 and Table S9). It has to be noted, however, that the HHTP emission is very weak, which is the reason for the large background in the TCSPC measurement (see Figure S13).

The TCSPC histogram and fit of solid powder **DPP2** are shown in Figure S14 and the corresponding short, medium, and long timescales τ_1, τ_2, and τ_3, respectively, can be found in Table S9. All three timescales are very similar to those of the crystalline **DPP2-HHTP-COF** emission at 620 nm, which we attribute to **DPP** stacks as part of the COF matrix. The only difference is in the fractional contributions, where τ_1 shows a smaller and τ_2 a larger contribution in the solid **DPP2** compared to the COF. For the solid **DPP2** precursor, τ_3 is larger than in the COF, but we note that they both lie within their combined error margins. These very similar characteristics support our assumption that the crystalline **DPP2-HHTP-COF** exhibits well-ordered **DPP2** stacks, showing a *J*-type interaction. Despite their similarity with respect to their error margins, a slightly reduced value for the **DPP2-HHTP-COF** singlet lifetime could originate from the interaction of the **DPP2** and **HHTP** molecules within the COF framework as next neighbors. While a reduced singlet lifetime has been observed upon COF formation, our study shows a relatively small change in singlet lifetime from aggregated **DPP2** to the **DPP2-HHTP COF**.[4]

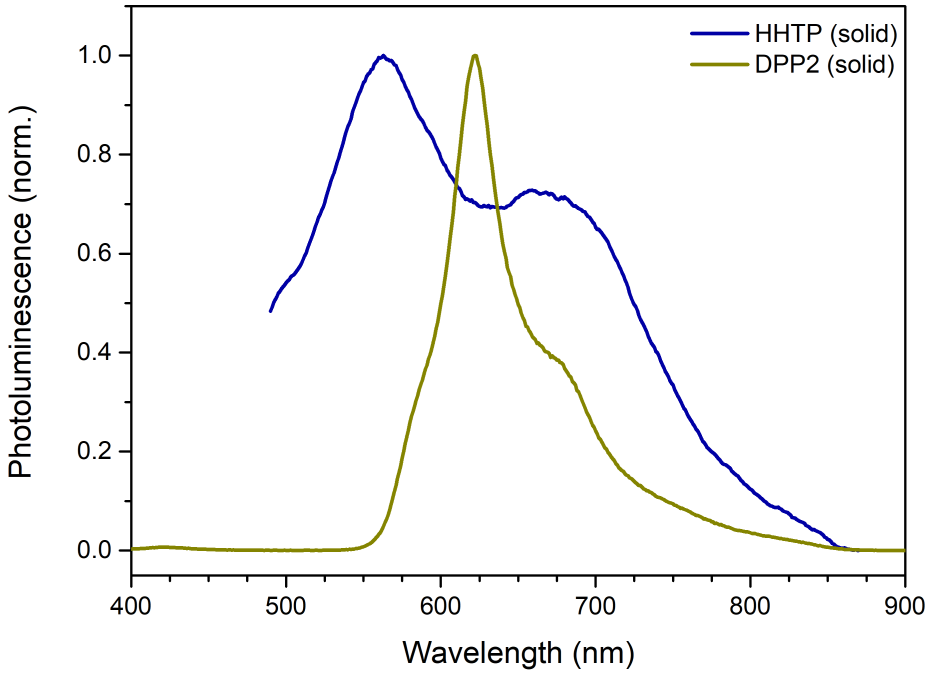

Fig. S12: Photoluminescence spectra of solid **DPP2** (green) and solid **HHTP** precursors (blue).

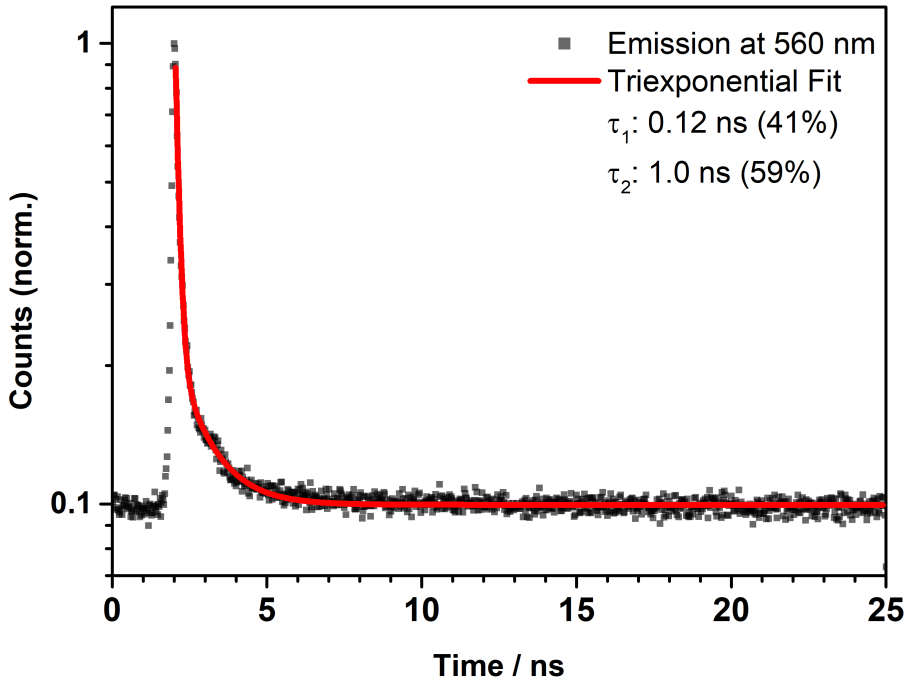

Fig. S13: TCSPC decay of neat **HHTP** in solid (powder) form at 560 nm (black squares) and a biexponential fit to the data (red line).

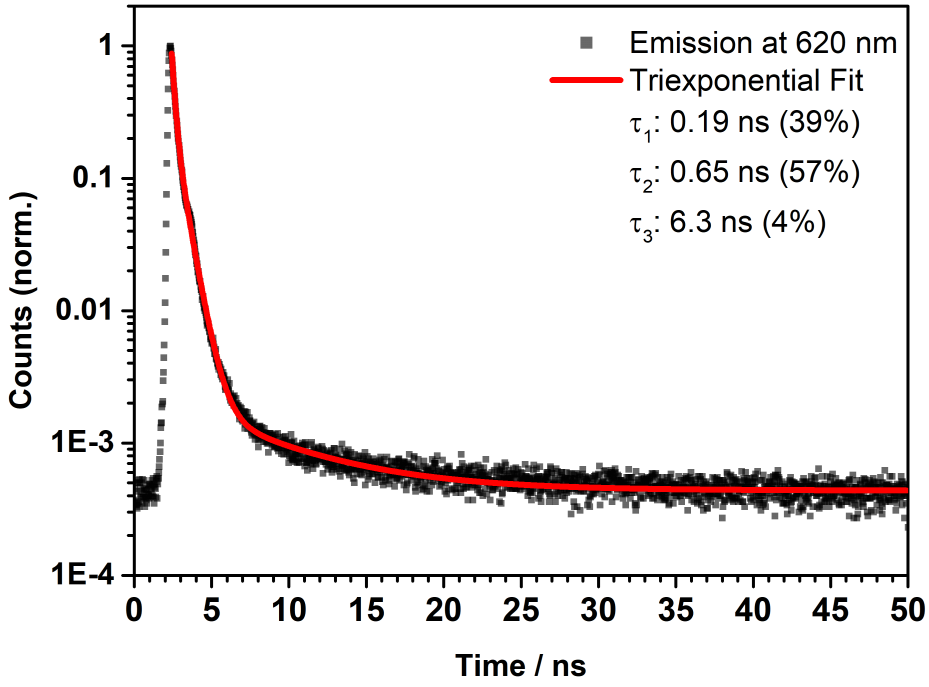

Fig. S14: TCSPC decay of neat **DPP2** in solid (powder) form at 620 nm (black squares) and a triexponential fit to the data (red line).

Table S9: Fitting results of the multiexponential fits to the respective TCSPC datasets of **HHTP** (see Figure S15) and solid **DPP2** (Figure S16). We note that uncertainties are fitting errors and, partly, much smaller than the instrument response of around 0.10 ns.

	DPP2 - solid	Fractional intensity	**HHTP** - solid	Fractional intensity
τ_1	(0.189 ± 0.004) ns	39%	(0.117 ± 0.005) ns	41%
τ_2	(0.647 ± 0.007) ns	57%	(1.04 ± 0.06) ns	59%
τ_3	(6.3 ± 0.5) ns	4%	-	-

9. XRD measurements

To obtain more (structural) information about the composition of our as-synthesized materials, different XRD measurements were performed. For this purpose, the crystalline COF, the amorphous COF and the **DPP2** precursor were placed on a silicon wafer and measured on a Bruker D8 diffractometer in reflection mode, respectively (start: 1.6 °2θ; end: 30 °2θ; step: 0.05 °; scan speed: 3 sec/step). The direct comparison between all three components is shown in Fig. S15 with logarithmic scale to visualize reflections even in high 2θ regions. Compared to the **DPP2** precursor data, the crystalline **DPP2-HHTP-COF** material is free of even small traces of (crystalline) impurities of the precursor. In addition, the amorphous material also does not correspond to the reflections of the **DPP2** precursor.

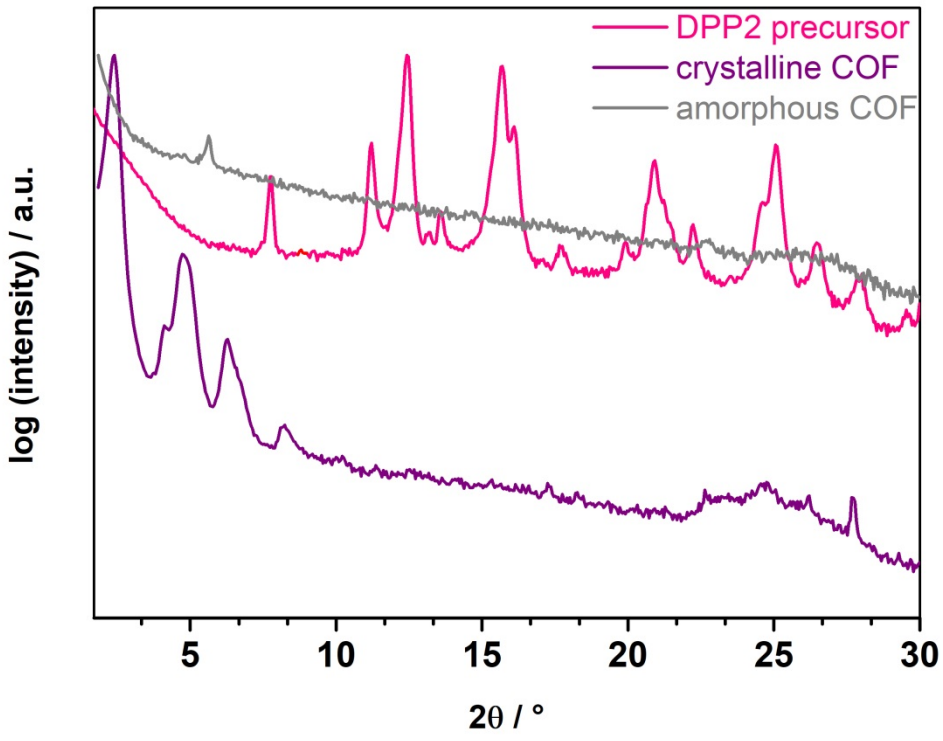

Fig. S15: PXRD measurements of crystalline **DPP2-HHTP COF** (purple), amorphous **DPP2-HHTP-COF** (grey) and aggregated **DPP2** solid precursor (pink); the amorphous phase shows no significant agreement with the crystalline material and the precursor, respectively. Please note the logarithmic scale of the intensity axis.

References

1. Huo, L.; Hou, J.; Chen, H.-Y.; Zhang, S.; Jiang, Y.; Chen, T. L.; Yang, Y., Bandgap and Molecular Level Control of the Low-Bandgap Polymers Based on 3,6-Dithiophen-2-yl-2,5-dihydropyrrolo[3,4-c]pyrrole-1,4-dione toward Highly Efficient Polymer Solar Cells. *Macromolecules* **2009,** 42, (17), 6564-6571.

2. Bürckstümmer, H.; Weissenstein, A.; Bialas, D.; Würthner, F., Synthesis and Characterization of Optical and Redox Properties of Bithiophene-Functionalized Diketopyrrolopyrrole Chromophores. *J. Org. Chem.* **2011,** 76, (8), 2426-2432.

3. Hestand, N. J.; Spano, F. C., Molecular Aggregate Photophysics beyond the Kasha Model: Novel Design Principles for Organic Materials. *Acc. Chem. Res.* **2017,** 50, (2), 341-350.

4. Keller, N.; Bessinger, D.; Reuter, S.; Calik, M.; Ascherl, L.; Hanusch, F. C.; Auras, F.; Bein, T., Oligothiophene-Bridged Conjugated Covalent Organic Frameworks. *J. Am. Chem. Soc.* **2017,** 139, (24), 8194-8199.